Geophysical Research Letters

RESEARCH LETTER
10.1029/2020GL090441

Large Atmospheric Waves Will Get Stronger, While Small Waves Will Get Weaker by the End of the 21st Century

R. Chemke[1] **and Y. Ming**[2]

[1]Department of Earth and Planetary Sciences, Weizmann Institute of Science, Rehovot, Israel, [2]NOAA/Geophysical Fluid Dynamics Laboratory, Princeton, NJ, USA

Key Points:

- By the end of the 21st century large tropical and midlatitudes waves will get stronger, while small waves will get weaker
- The opposite response of large and small waves to anthropogenic emissions stems from the waves' opposite growth rate response
- Studying future wave changes by pooling all scales together masks the different climate impacts of large and small waves

Supporting Information:

- Supporting Information S1

Correspondence to:
R. Chemke,
rei.chemke@weizmann.ac.il

Citation:
Chemke, R., & Ming, Y. (2020). Large atmospheric waves will get stronger, while small waves will get weaker by the end of the 21st century. *Geophysical Research Letters*, *47*, e2020GL090441. https://doi.org/10.1029/2020GL090441

Received 19 AUG 2020
Accepted 1 NOV 2020
Accepted article online 4 NOV 2020

Abstract Atmospheric waves control the weather and climate variability, by affecting winds, temperature, and precipitation. It is thus critical to assess their future response to anthropogenic emissions. Most previous studies investigated the projected regional changes in the intensity of atmospheric waves, by pooling across waves with different scales. However, the waves' projected changes might vary with their scale, and thus, their future climate impacts might also be scale dependent. Here we show that both in the tropics and midlatitudes while large waves will get stronger, small waves will get weaker by the end of this century. Thus, investigating the response of atmospheric waves to human activity by pooling across all wave scales masks the future climate impacts of large waves. We further reveal that the opposite response of large and small waves stems from the opposite effect of static stability and zonal wind on the growth rate of the different waves.

1. Introduction

Atmospheric waves play a central role in shaping the weather and climate on Earth. Not only that atmospheric waves affect the daily to monthly weather variability, by modulating winds, temperature, and precipitation (e.g., midlatitude storms), they also affect Earth's climate by transferring heat, momentum, and moisture across latitudes and longitudes. Thus, even modest changes in these waves could have large global climate impacts (Held, 1993).

By the end of this century climate models project an intensification of midlatitudes storms in the Southern Hemisphere winter, a reduction in Northern Hemisphere summer, and no robust changes in the storms' overall intensity during Northern Hemisphere winter and Southern Hemisphere summer (partly due to the poleward of shift of the storm tracks) (E. K. M. Chang et al., 2012; Harvey et al., 2014; Lehmann et al., 2014; O'Gorman, 2010). Some of these changes have already been observed over recent decades (Coumou et al., 2015). In the tropics, the Madden-Julian Oscillation (MJO, the largest intraseasonal variability in the tropics) amplitude is projected to increase (Adames et al., 2017; Bui & Maloney, 2018; C. J. Chang et al., 2015; Rushley et al., 2019; Subramanian et al., 2014); however, there are large differences in the reported enhancements (Bui & Maloney, 2018; Maloney et al., 2019).

Since the intensity of atmospheric waves varies with their scale, the climate effects of the waves' response to anthropogenic emissions might also vary with scale; that is, not necessarily, the atmospheric waves' response to anthropogenic emissions occurs uniformly across all scales. For example, previous studies, which analyzed associated metrics of wave activity (e.g., the meridional wind and Northern Hemisphere geopotential height), showed that in the upper troposphere at midlatitudes while amplitudes of long wavelengths are projected to increase, their short wavelength amplitudes are projected to decrease (Kidston et al., 2011; Rivière, 2011; Sussman et al., 2020). Whether such changes occur when accounting for the total wave energy, all atmospheric levels, and different regions is still an open question.

Furthermore, the underlying mechanism of the projected changes of atmospheric waves in spectral space is not fully understood. The above scale-dependent wave response might be linked to the projected increase in the eddy length scale (i.e., the scale that holds most of the energy, Kidston et al., 2010). Previous studies have suggested that an increase in the eddy length scale might stem from increases in static stability and tropopause height (Kidston et al., 2010; Williams, 2006), via their effect on the Rossby deformation radius. However, a significant correlation between the projected changes in eddy length scale and static stability only appears in the Southern Hemisphere, while the above scale-dependent wave response was reported in

both hemispheres (Kidston et al., 2010, 2011); several previous studies showed that the deformation radius does not capture the most unstable wavenumber or the eddy length scale (Chemke & Kaspi, 2015; Chemke et al., 2016; Frierson et al., 2006). In addition, changes in upper tropospheric wind shear were also argued to explain the increase in the eddy length scale, as they have opposite effects on the stability of short and long waves (Rivière, 2011). To date, the relative roles of the above variables in the future scale-dependent wave response have not been assessed in fully coupled models. In this work we address the above open questions by conducting a spectral analysis on the future changes in atmospheric waves in order to better understand their projected climate impacts.

2. Methods

2.1. CMIP5 Models

We use daily output of zonal and meridional winds, geopotential height, and temperature from 15 models that participate in the Coupled Model Intercomparison Project Phase 5 (CMIP5) (Taylor et al., 2012) and select only the "r1i1p1" member between 1850 and 2100 with the Historical (through 2005) and Representative Concentration Pathway 8.5 (RCP8.5, through 2100) experiments (supporting information Table S1), in order to weigh all models equally. As discussed throughout the text, all figures below are plotted using annual mean values, and the seasonality of the analysis is shown in the supporting information.

2.2. EKE

The eddy kinetic energy (EKE) per unit mass is defined as

$$\mathrm{EKE} = \frac{1}{2}(u'^2 + v'^2), \tag{1}$$

where u is the zonal wind, v is the meridional wind, and prime denotes deviation from zonal mean. The EKE is calculated daily thus includes both transient and stationary waves. We follow previous studies (Lambert, 1984) and calculate the 2-D spectrum of the EKE using the vorticity and divergence. The integrated EKE over the atmospheric mass per unit area, dm, can be written using the stream function, ψ, and the velocity potential, χ, as follows:

$$\int \frac{1}{2}(u'^2 + v'^2)dm = -\frac{1}{2}\int \psi'\nabla^2\psi' + \chi'\nabla^2\chi' dm, \tag{2}$$

where $\int dm = \frac{1}{4\pi g}\int_0^{p_s}\int_0^{2\pi}\int_{-\pi/2}^{\pi/2}\cos\phi d\phi d\lambda dp$, p_s is surface pressure, g is gravity, and $\zeta' = \nabla^2\psi'$ and $D' = \nabla^2\chi'$ are the eddy components of the vorticity and divergence, respectively. Using spherical harmonics as basis functions, and recalling that $\{\nabla^2 A\}_{n,k} = -\frac{n(n+1)}{a^2}A_{n,k}$, where n and k are the total and zonal wavenumbers, respectively, and a is Earth's radius, the EKE can be written in spectral space as follows:

$$\mathrm{EKE_n} = \frac{1}{4g}\int_0^{p_s}\sum_{k=-n}^{n}\frac{a^2}{n(n+1)}(|D'_{n,k}|^2 + |\zeta'_{n,k}|^2)dp. \tag{3}$$

Finally, the zonal EKE spectrum is computed using a one-dimensional Fourier analysis at each latitude (Saltzman, 1957):

$$\mathrm{EKE_k} = \frac{1}{g}\int_0^{p_s}|u'_k|^2 + |v'_k|^2 dp. \tag{4}$$

2.3. Spectral EKE Budget

To better elucidate the changes in the zonal EKE spectrum at midlatitudes, we follow previous studies (Chemke, 2017; Chemke et al., 2016; Chemke & Kaspi, 2015; Saltzman, 1957) and analyze the EKE budget:

$$\frac{\partial \mathrm{EKE_k}}{\partial t} = \mathrm{PK} + \mathrm{EM} + \mathrm{EE} + \mathrm{F}, \tag{5}$$

where

$$\mathrm{PK} = -\frac{2}{g}\int_0^{p_s}\mathrm{Re}\left\{\mathbf{u}'^*_k \cdot \nabla\varphi'_k\right\} dp, \tag{6}$$

contains the generation of EKE (the conversion from eddy available potential energy to EKE), where $\mathbf{u}$ denotes the horizontal velocity vector, the asterisk denotes a complex conjugate, and φ is the geopotential:

$$\mathrm{EM} = -\frac{2}{g}\int_0^{p_s} \mathrm{Re}\left\{ u_k'^{*}\left(\overline{\mathbf{u}}\cdot\nabla u' + \mathbf{u}'\cdot\nabla\overline{u} - \frac{\overline{u}v'\tan\phi}{a} - \frac{u'\overline{v}\tan\phi}{a}\right)_k + v_k'^{*}\left(\overline{\mathbf{u}}\cdot\nabla v' + \mathbf{u}'\cdot\nabla\overline{v} + 2\frac{\overline{u}u'\tan\phi}{a}\right)_k \right\} dp, \tag{7}$$

contains the wave-mean interactions (the transfer of energy between the waves and the zonal mean flow), where overbar denotes a zonal mean:

$$\mathrm{EE} = -\frac{2}{g}\int_0^{p_s} \mathrm{Re}\left\{ u_k'^{*}\left(\mathbf{u}'\cdot\nabla u' - \frac{u'v'\tan\phi}{a}\right)_k + v_k'^{*}\left(\mathbf{u}'\cdot\nabla v' + \frac{u'u'\tan\phi}{a}\right)_k \right\} dp, \tag{8}$$

contains the wave-wave interactions (the transfer of energy between the different waves), and F contains dissipation processes. Since F is not available from CMIP5 models, and in order to close the budget, it is calculated as the residual between the EKE tendency ($\frac{\partial EKE_k}{\partial t}$) and PK, EM, and EE.

2.4. Linear Normal Mode Instability Analysis

For calculating the growth rate of the waves, which represents the extraction of mean potential energy, we follow previous studies (Chemke, 2017; Chemke et al., 2016; Chemke & Kaspi, 2015, 2016a, 2016b; Chemke & Polvani, 2019; Smith, 2007) and conduct a linear normal-mode instability analysis to the quasigeostrophic equations (simplified equations for the midlatitude flow). The quasigeostrophic equations (conservation of interior quasigeostrophic potential vorticity and buoyancy at the vertical boundaries) linearized about the midlatitude mean state, can be written as follows:

$$\begin{aligned} &\frac{\partial q'}{\partial t} + \tilde{\overline{\mathbf{u}}}\cdot\nabla q' + \mathbf{u}'\cdot\nabla\tilde{\overline{q}} = 0, H_p < p < p_s \\ &\frac{\partial}{\partial t}\frac{\partial\psi'}{\partial p} + \tilde{\overline{\mathbf{u}}}\cdot\nabla\frac{\partial\psi'}{\partial p} + \mathbf{u}'\cdot\nabla\frac{\partial\tilde{\overline{\psi}}}{\partial p} = 0, p = H_p, p_s, \end{aligned} \tag{9}$$

where $q' = \nabla^2\psi' + \Gamma\psi'$ is the eddy quasigeostrophic potential vorticity, $\Gamma = \frac{\partial}{\partial p}\frac{f^2}{S^2}\frac{\partial}{\partial p}$, $S^2 = -\frac{1}{\tilde{\overline{\rho}}\tilde{\overline{\theta}}}\frac{\partial\tilde{\overline{\theta}}}{\partial p}$ is static stability, θ is potential temperature, ρ is the density, and tilde represents time and midlatitude mean (averaged over 30–60° and over the last 20 years of either the 20th or 21st century, i.e., the mean fields are only a function of pressure). $\nabla\tilde{\overline{q}} = \Gamma\tilde{\overline{v}}\hat{i} + (\beta - \Gamma\tilde{\overline{u}})\hat{j}$ is the mean quasigeostrophic potential vorticity gradient, β is the meridional derivative of the Coriolis parameter, H_p is the tropopause height (defined, following the World Meteorological Organization, as the lowest level where the vertical temperature gradient crosses the 2 K km^{-1} value), and $\nabla\frac{\partial\tilde{\overline{\psi}}}{\partial p} = \frac{\partial\tilde{\overline{v}}}{\partial p}\hat{i} - \frac{\partial\tilde{\overline{u}}}{\partial p}\hat{j}$.

Substituting a plane wave solution, $\psi' = \mathrm{Re}\left\{\hat{\psi}'(p)e^{i(kx-\omega t)}\right\}$, where ω is frequency, into Equation 9 yields an eigenvalue problem for the normal modes $\hat{\psi}'$. A nonzero imaginary component of the eigenvalues, ω, thus represents an exponential growth of the solution (i.e., the growth rate of the waves). We numerically solve the resulting eigenvalue problem using the mean fields (velocity, temperature, and tropopause height) from each of the CMIP5 models and investigate the growth rate of the most unstable normal mode. Lastly, the equation is solved for an infinitely wide channel (i.e., for a zero meridional wavenumber).

3. Future Changes in EKE

We start by considering the waves' global response. This is done by computing the spectrum of the column integrated EKE using spherical harmonics as basis functions (Baer, 1972; Boer & Shepherd, 1983; Lambert, 1984); EKE is a widely used measure for the intensity of atmospheric waves. Note that while one would not fully elucidate the climate impacts of atmospheric waves via spherical harmonics decomposition, as it pools waves across different regions on Earth, such decomposition provides basic understanding in the behavior of atmospheric waves. Figure 1a shows the climatology (average over the 1980–1999 period) of annual mean EKE spectrum as a function of total wavenumber in 15 CMIP5 models. The EKE peaks around total wavenumbers 6–10 since most of the EKE resides in midlatitudes; midlatitude waves typically have zonal wavenumbers 3–6 and the large EKE values at midlatitudes result in meridional wavenumbers 3–4.

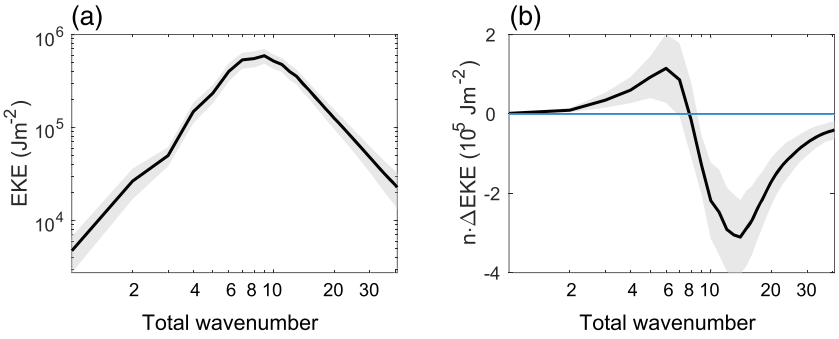

Figure 1. The eddy kinetic energy as a function of total wavenumber in (a) climatology and (b) response to anthropogenic emissions. The solid black line shows the CMIP5 mean and the shading one standard deviations across CMIP5 models. The response is multiplied by the wavenumber (to preserve the integral on the semilogarithmic axes) and smoothed with a 3-point running mean for plotting purposes.

The future response of the EKE to anthropogenic emissions (the difference between the 2080–2099 and 1980–1999 periods) is opposite for large and small waves (Figure 1b): Large waves (small wavenumbers) will get stronger, while small waves (large wavenumbers) will get weaker. Furthermore, while these scale-dependent EKE changes are mostly associated with transient waves (timescales smaller than one month), they also appear in stationary waves (timescales larger than 1 month) (supporting information Figure S1). Note that the overall weakening of small waves is larger than the strengthening of large waves; thus, integrating over all wavenumbers yields a projected global EKE decline of ~2% ($-1.8 \cdot 10^5\,\mathrm{J\,m^{-2}}$). Clearly, this total response of the atmospheric waves masks the different future climate effects of large and small waves (e.g., while wavenumbers 1–6 increase by ~8%, wavenumbers 11–16 decrease by ~6.5%). This emphasizes the importance of studying the waves' response to anthropogenic emissions as a function of the waves' scale. We focus here on the annual mean since the waves' response as a function of wavenumber is similar in all seasons (supporting information Figure S2).

To further elucidate the climate impacts of the "large-get-stronger, small-get-weaker" wave response, it is instructive to investigate in which regions this interesting pattern emerges. This is done by computing at each latitude the one-dimensional Fourier spectrum of EKE (Chemke, 2017; Chemke et al., 2016; Chemke & Kaspi, 2015; Saltzman, 1957) and averaging over three regions (pooling both hemispheres): tropics (0–30°), midlatitudes (30–60°), and polar regions (60–90°). Figure 2a shows the climatology of annual mean EKE spectrum as a function of zonal wavenumber in the tropics (red), midlatitudes (blue), and polar regions (yellow). Unlike the global spectrum in Figure 1a, the zonal spectrum shows that the intensity of atmospheric waves increases with the waves' zonal scale, due to the presence of large planetary waves.

The "large-get-stronger, small-get-weaker" wave response is mostly apparent at midlatitudes (blue), to a lesser extent at the tropics (red), and it is not apparent at polar regions (yellow) (Figure 2b). As noted above, studying the total response of the waves (as was previously done), rather their scale-dependent response, at each region obscures the climate impacts of the different waves. In particular, it obscures the expected

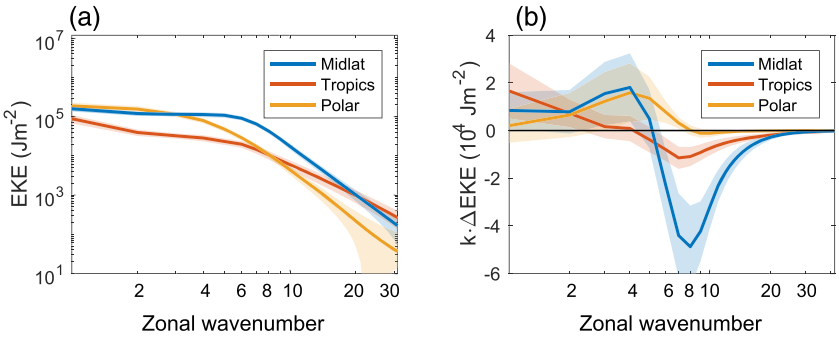

Figure 2. As in Figure 1 but for the eddy kinetic energy as a function of zonal wavenumber in midlatitudes (blue), tropics (red), and polar regions (yellow).

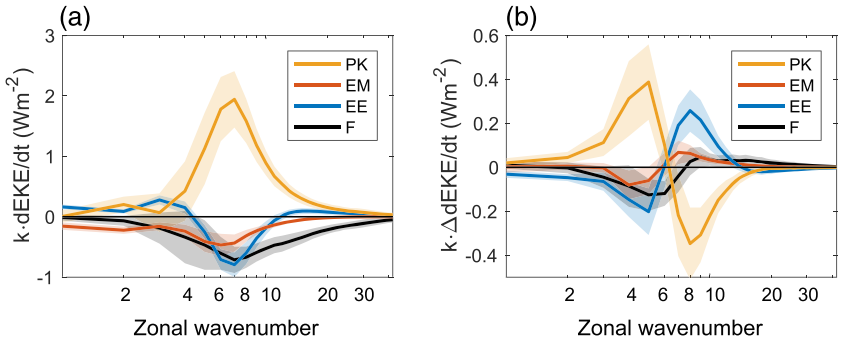

Figure 3. Components of the eddy kinetic energy budget as a function of zonal wavenumber in (a) climatology and (b) response to anthropogenic emissions. Yellow, red, blue, and black lines show the conversion of eddy potential energy to EKE (PK), transfer of kinetic energy between the waves and the mean flow (EM), transfer of EKE between the different waves (EE), and dissipation (F), respectively. The solid lines show the CMIP5 mean and the shading one standard deviations across CMIP5 models. The components are multiplied by the wavenumber (to preserve the integral on the semilogarithmic axes).

increase in the climate impacts of large waves. We average here each region over both hemispheres as the annual mean response of the EKE zonal spectrum in each hemisphere shows the same behavior over all three regions (supporting information Figure S3). In addition, we again focus on the annual mean EKE response since the scale-dependent EKE changes at each region occur through all seasons, except for Northern Hemisphere summer (supporting information Figures S4 and S5). The opposite response of large and small midlatitudes waves during Northern Hemisphere winter and Southern Hemisphere summer might explain part of the previously reported insignificant changes in midlatitudes waves intensity, which accounted for both large and small waves (E. K. M. Chang et al., 2012; Harvey et al., 2014; Lehmann et al., 2014).

Similar to the changes in the global spectrum and to changes in Northern Hemisphere midlatitudes 500 hPa geopotential height (Sussman et al., 2020), at midlatitudes most of the "large-get-stronger, small-get-weaker" wave response stems from transient waves, with a small contribution from stationary waves (supporting information Figures S1c and S1d). This suggests that baroclinic instability, which drives transient midlatitude waves, might play an important role in the scale-dependent EKE changes at midlatitudes (as shown below). In the tropics, however, transient and stationary waves play a comparable role in the "large-get-stronger, small-get-weaker" wave response (supporting information Figure S1), suggesting that different types of tropical waves (i.e., waves with different dispersion relations) account for the tropical wave response. Interestingly, while such scale-dependent wave responses in the tropics have not been observed over recent decades, a frequency-dependent wave response has been documented (Raghavendra et al., 2019).

4. The Source of Scale-Dependent EKE Changes

Since the scale-dependent wave response is mostly apparent at midlatitudes, and given that many characteristics of tropical waves are not well simulated in CMIP5 models (Ahn et al., 2017; Jiang et al., 2015), we next focus on midlatitudes and investigate which physical process is responsible for the waves' response. This is done by analyzing the spectral EKE budget at midlatitudes (Chemke, 2017; Chemke et al., 2016; Chemke & Kaspi, 2015; Saltzman, 1957). The EKE budget takes a simple form (Equation 5), where four processes affect the EKE: conversion of eddy potential energy to EKE (PK), transfer of kinetic energy between the zonal mean flow (the zero zonal wavenumber) and the waves (EM), transfer of EKE between the different waves (EE), and dissipation (F).

The climatology of these four processes is shown in Figure 3a, where positive values indicate EKE gain and negative values EKE loss. First, the waves gain their kinetic energy via the conversion of eddy potential energy to EKE, which peaks around zonal wavenumbers 5–7 (Simmons & Hoskins, 1978) (PK, yellow line). This conversion is part of baroclinic instability, a process that give rise to atmospheric perturbations at midlatitudes (e.g., weather systems) via the extraction of potential energy from the mean atmospheric state (i.e., a rotating stably stratified fluid with a poleward decline in temperature) (Charney, 1947; Eady, 1949; Vallis, 2006). Second, the EKE gain across all wavenumbers is balanced by EKE loss from two processes:

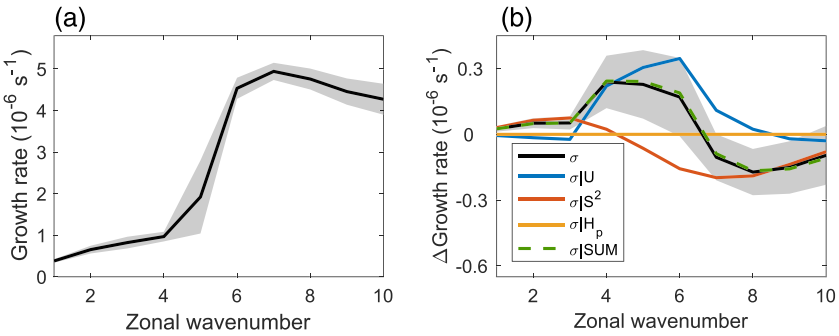

Figure 4. The growth rate of midlatitude waves based on the linear normal-mode instability analysis in (a) climatology and (b) response to anthropogenic emissions (black). Blue, red, and yellow lines, respectively, show the contributions of the mean zonal wind (U), static stability (S^2), and tropopause height (H_p) to the growth rate response. Dashed green line shows the sum from all contributions. The solid lines show the CMIP5 mean and the shading one standard deviations across CMIP5 models. The response is smoothed with a 3-point running mean for plotting purposes.

energy transfer from the waves to the mean flow (EM, red line) and dissipation of energy (F, black line). Third, the EKE gain around wavenumber 6 is also partly balanced by the interactions between the waves, which transfer energy from wavenumbers 5–10 mostly upscale to wavenumbers 1–4 (EE, blue line). This process, known as inverse energy cascade, is a characteristic of two-dimensional turbulent flow, a flow that many of its features can be found in the midlatitude atmosphere (Charney, 1971; Chemke, 2017; Chemke & Kaspi, 2015; Chemke et al., 2016; Rhines, 1977; Salmon, 1978).

The future response of the EKE budget, shown in Figure 3b, reveals that the term that mostly contributes to the strengthening of large waves and weakening of small waves is the conversion of eddy potential to kinetic energy (PK, yellow line). Thus, the "large-get-stronger, small-get-weaker" wave response is a result of changes in the extraction of mean potential energy by the waves. All other terms exhibit an opposite response: They remove energy from large waves and add energy to small waves. This is mostly evident in the EKE transfer between the different waves (EE, blue line), which suggests a weakening in the inverse energy cascade at midlatitudes (Chemke, 2017).

Finally, to better elucidate the source of the scale-dependent changes in the conversion of eddy potential to kinetic energy, we follow previous studies and conduct a linear normal-mode instability analysis (Chemke, 2017; Chemke et al., 2016; Chemke & Kaspi, 2015, 2016a, 2016b; Chemke & Polvani, 2019; Smith, 2007; Rivière, 2011). This is done by numerically solving an eigenvalue problem for a simplified equation for the midlatitude flow (the linearized quasigeostrophic equation, Equation 9) in order to explore the growth rate of the waves (the eigenvalues); the growth rate represents the extraction of mean potential energy by the waves. The equation is solved for the first 10 zonal wavenumbers (where the simplified equation is expected to hold) over the 2080–2099 and 1980–1999 periods using the models' mean zonal wind, static stability, and tropopause height. Figure 4a shows the climatology of the waves' growth rate as function of the zonal wavenumber. As expected from linear baroclinic instability theory (Eady, 1949), the growth rate of large waves peaks around zonal wavenumbers 5–7, in accordance with the climatology of the conversion of eddy potential energy to EKE (yellow line in Figure 3a).

In spite of simplifying the midlatitude flow to an eigenvalue problem, the projected response of the growth rate is overall similar to the response of the conversion of eddy potential to kinetic energy and to the response of midlatitudes EKE: The growth rate is projected to increase at wavenumbers 1–5 and decrease at wavenumbers 6–8 (black line in Figure 4b). Thus, large waves are projected to become more unstable and extract more mean potential energy (EKE increase), while short waves are projected to become less unstable, and extract less energy from the mean flow (EKE decline).

To better understand the growth rate response, we calculate the relative contribution of each of the input variables (mean zonal wind, static stability, and tropopause height) to the growth rate response. This is done by re-solving the eigenvalue problem with all input variables set to the 1980–1999 period, except for one; the difference between the resulting growth rates and the growth rate of the 1980–1999 period (Figure 4a) isolates the relative contribution of each variable to the projected growth rate response. The sum from all

contributions is very similar to the growth rate response (cf. dashed green and black lines), which allows us to quantify their relative importance.

Changes in static stability (red) and mean zonal wind (blue) explain most of the increase in the growth rate of large scales and the decrease in the growth rate of smaller scales. On the other hand, changes in the tropopause height (yellow) have minor contributions to the growth rate response. The effect of the mean zonal wind on the growth rate response was argued to stem from an increase in upper tropospheric wind shear (equivalent to an increase in the meridional temperature gradient), rather than lower tropospheric wind shear (Rivière, 2011). Thus, the projected tropical upper tropospheric warming (a consequence of a reduction in the moist adiabatic lapse rate), which acts to both stabilize the troposphere (increase the static stability) and increase the meridional temperature gradient aloft (supporting information Figure S6), seems to play an important role in the projected "large-get-stronger, small-get-weaker" wave response. This adds to the recent findings on the importance of upper tropospheric warming in modulating midlatitudes EKE (Shen & Ming, 2018; Yuval & Kaspi, 2020). Note that since models were found to overestimate the recent tropical upper tropospheric warming (e.g., Fu et al., 2011; Mitchell et al., 2013; Po-Chedley & Fu, 2012; Seidel et al., 2012), it is conceivable that the simulated projected tropical upper tropospheric warming is also biased, which thus might affect the magnitude of the projected "large-get-stronger, small-get-weaker" wave response.

5. Conclusions

Most previous studies who investigated the future response of atmospheric waves to anthropogenic emissions have focused on the total wave response (i.e., pooling across all waves with different scales). This study shows, however, that the future response of atmospheric waves to anthropogenic emissions is opposite for large and small waves in the tropics and midlatitudes: While large waves are projected to get stronger, small waves are projected to get weaker. We here extend the work of previous studies, which showed similar spectral changes in associated metrics of wave activity in the upper troposphere at midlatitudes, and investigate the spectral changes in total wave activity, accounting for all atmospheric levels and all latitude bands. Our analysis thus not only reveals new aspects of the projected climate impacts of atmospheric waves—namely, an expected increase in the climate impacts of large waves—but also shed new light on previously reported atmospheric waves changes. We show that the insignificant future changes in the intensity of midlatitudes waves during Northern Hemisphere winter and Southern Hemisphere summer are partly due to a cancelation between the large and small waves' opposite responses. Thus, in order to increase the effectiveness of climate change adaptation strategies, the future climate impacts of atmospheric waves should be investigated as a function of their scale.

Data Availability Statement

The CMIP5 data are available online (at https://esgf-node.llnl.gov/projects/cmip5/).

Acknowledgments
R. C. is grateful to Lorenzo Polvani for his support and fruitful discussions.

References

Adames, A. F., Kim, D., Sobel, A. H., Del Genio, A., & Wu, J. (2017). Changes in the structure and propagation of the MJO with increasing CO_2. *Journal of Advances in Modeling Earth Systems*, *9*, 1251–1268. https://doi.org/10.1002/2017MS000913

Ahn, M., Kim, D., Sperber, K. R., Kang, I., Maloney, E., Waliser, D., & Hendon, H. (2017). MJO simulation in CMIP5 climate models: MJO skill metrics and process-oriented diagnosis. *Climate Dynamics*, *49*(11–12), 4023–4045.

Baer, F. (1972). An alternate scale representation of atmospheric energy spectra. *Journal of the Atmospheric Sciences*, *29*(4), 649–664.

Boer, G. J., & Shepherd, T. G. (1983). Large-scale two-dimensional turbulence in the atmosphere. *Journal of the Atmospheric Sciences*, *40*(1), 164–184.

Bui, H. X., & Maloney, E. D. (2018). Changes in Madden-Julian Oscillation precipitation and wind variance under global warming. *Geophysical Research Letters*, *45*, 7148–7155. https://doi.org/10.1029/2018GL078504

Chang, E. K. M., Guo, Y., & Xia, X. (2012). CMIP5 multimodel ensemble projection of storm track change under global warming. *Journal of Geophysical Research*, *117*, D23118. https://doi.org/10.1029/2012JD018578

Chang, C. J., Tseng, W., Hsu, H., Keenlyside, N., & Tsuang, B. (2015). The Madden-Julian Oscillation in a warmer world. *Geophysical Research Letters*, *42*, 6034–6042. https://doi.org/10.1002/2015GL065095

Charney, J. G. (1947). The dynamics of long waves in a baroclinic westerly current. *Journal of Meteorology*, *4*(5), 136–162.

Charney, J. G. (1971). Geostrophic turbulence. *Journal of the Atmospheric Sciences*, *28*(6), 1087–1095.

Chemke, R. (2017). Atmospheric energy transfer response to global warming. *Quarterly Journal of the Royal Meteorological Society*, *143*, 2296–2308. https://doi.org/10.1002/qj.3086

Chemke, R., Dror, T., & Kaspi, Y. (2016). Barotropic kinetic energy and enstrophy transfers in the atmosphere. *Geophysical Research Letters*, *43*, 7725–7734. https://doi.org/10.1002/2016GL070350

Chemke, R., & Kaspi, Y. (2015). The latitudinal dependence of atmospheric jet scales and macroturbulent energy cascades. *Journal of the Atmospheric Sciences*, *72*(10), 3891–3907.
Chemke, R., & Kaspi, Y. (2016a). The effect of eddy-eddy interactions on jet formation and macroturbulent scales. *Journal of the Atmospheric Sciences*, *73*(5), 2049–2059.
Chemke, R., & Kaspi, Y. (2016b). The latitudinal dependence of the oceanic barotropic eddy kinetic energy and macroturbulence energy transport. *Geophysical Research Letters*, *43*, 2723–2731. https://doi.org/10.1002/2016GL067847
Chemke, R., & Polvani, L. M. (2019). Exploiting the abrupt 4xCO_2 scenario to elucidate tropical expansion mechanisms. *Journal of Climate*, *32*(3), 859–875. https://doi.org/10.1175/JCLI-D-18-0330.1
Coumou, D., Lehmann, J., & Beckmann, J. (2015). The weakening summer circulation in the Northern Hemisphere mid-latitudes. *Science*, *348*(6232), 324–327.
Eady, E. T. (1949). Long waves and cyclone waves. *Tellus*, *1*(3), 33–52.
Frierson, D. M. W., Held, I. M., & Zurita-Gotor, P. (2006). A gray-radiation aquaplanet moist GCM. Part I: Static stability and eddy scale. *Journal of the Atmospheric Sciences*, *63*(10), 2548–2566.
Fu, Q., Manabe, S., & Johanson, C. M. (2011). On the warming in the tropical upper troposphere: Models versus observations. *Geophysical Research Letters*, *38*(15), L15704. https://doi.org/10.1029/2011GL048101
Harvey, B. J., Shaffrey, L. C., & Woollings, T. J. (2014). Equator-to-pole temperature differences and the extra-tropical storm track responses of the CMIP5 climate models. *Climate Dynamic*, *43*(5–6), 1171–1182.
Held, I. M. (1993). Large-scale dynamics and global warming. *Bulletin of the American Meteorological Society*, *74*, 228–242.
Jiang, X., Waliser, D. E., Xavier, P. K., Petch, J., Klingaman, N. P., Woolnough, S. J., et al. (2015). Vertical structure and physical processes of the Madden-Julian oscillation: Exploring key model physics in climate simulations. *Journal of Geophysical Research: Atmospheres*, *120*, 4718–4748. https://doi.org/10.1002/2014JD022375
Kidston, J., Dean, S. M., Renwick, J. A., & Vallis, G. K. (2010). A robust increase in the eddy length scale in the simulation of future climates. *Geophysical Research Letters*, *37*, L03806. https://doi.org/10.1029/2009GL041615
Kidston, J., Vallis, G. K., Dean, S. M., & Renwick, J. A. (2011). Can the increase in the eddy length scale under global warming cause the poleward shift of the jet streams?. *Journal of Climate, 24*(14), 3764–3780.
Lambert, S. J. (1984). A global available potential energy-kinetic energy budget in terms of the two-dimensional wavenumber for the FGGE year. *Atmosphere-Ocean*, *22*(3), 265–282.
Lehmann, J., Coumou, D., Frieler, K., Eliseev, A. V., & Levermann, A. (2014). Future changes in extratropical storm tracks and baroclinicity under climate change. *Environmental Research Letters*, *9*(8), 84002.
Maloney, E. D., Adames, A. F., & Bui, H. X. (2019). Madden-Julian oscillation changes under anthropogenic warming. *Nature Climate Change*, *9*(1), 26–33.
Mitchell, D. M., Thorne, P. W., Stott, P. A., & Gray, L. J. (2013). Revisiting the controversial issue of tropical tropospheric temperature trends. *Geophysical Research Letters*, *40*, 2801–2806. https://doi.org/10.1002/grl.50465
O'Gorman, P. A. (2010). Understanding the varied response of the extratropical storm tracks to climate change. *Proceedings of the National Academy of Sciences of the United States of America*, *107*, 19,176–19,180.
Po-Chedley, S., & Fu, Q. (2012). Discrepancies in tropical upper tropospheric warming between atmospheric circulation models and satellites. *Environmental Research Letters*, *7*(4), 044018. https://doi.org/10.1088/1748-9326/7/4/044018
Raghavendra, A., Roundy, P. E., & Zhou, L. (2019). Trends in tropical wave activity from the 1980s to 2016. *Journal of Climate*, *32*(5), 1661–1676.
Rhines, P. B. (1977). *The dynamics of unsteady currents*. In E. D. Goldberg (Eds.), (Vol. VI, pp. 189–318). New York, US: John Wiley and Sons, Inc.
Rivière, G. (2011). A dynamical interpretation of the poleward shift of the jet streams in global warming scenarios. *Journal of the Atmospheric Sciences*, *68*, 1253–1272.
Rushley, S. S., Kim, D., & Adames, A. F. (2019). Changes in the MJO under greenhouse gas-induced warming in CMIP5 models. *Journal of Climate*, *32*(3), 803–821.
Salmon, R. (1978). Two-layer quasi-geostrophic turbulence in a simple special case. *Geophysical & Astrophysical Fluid Dynamics*, *10*(1), 25–52.
Saltzman, B. (1957). Equations governing the energetics of the larger scales of atmospheric turbulence in the domain of wave number. *Journal of Meteorology*, *14*(6), 513–523.
Seidel, D. J., Free, M., & Wang, J. S. (2012). Reexamining the warming in the tropical upper troposphere: Models versus radiosonde observations. *Geophysical Research Letters*, *39*, L22701. https://doi.org/10.1029/2012GL053850
Shen, Z., & Ming, Y. (2018). The influence of aerosol absorption on the extratropical circulation. *Journal of Climate*, *31*(15), 5961–5975.
Simmons, A. J., & Hoskins, B. J. (1978). The life cycles of some nonlinear baroclinic waves. *Journal of the Atmospheric Sciences*, *35*(3), 414–432.
Smith, K. S. (2007). The geography of linear baroclinic instability in Earth's oceans. *Journal of Marine Research*, *65*(5), 655–683.
Subramanian, A., Jochum, M., Miller, A. J., Neale, R., Seo, H., Waliser, D., & Murtugudde, R. (2014). The MJO and global warming: A study in CCSM4. *Climate Dynamics*, *42*(7–8), 2019–2031.
Sussman, H. S., Raghavendra, A., Roundy, P. E., & Dai, A. (2020). Trends in northern midlatitude atmospheric wave power from 1950 to 2099. *Climate Dynamics*, *54*(5–6), 2903–2918.
Taylor, K. E., Stouffer, R. J., & Meehl, G. A. (2012). An overview of CMIP5 and the experiment design. *Bulletin of the American Meteorological Society*, *93*, 485–498.
Vallis, G. K. (2006). *Atmospheric and oceanic fluid dynamics* (p. 770). Cambridge, UK: Cambridge University Press.
Williams, G. P. (2006). Circulation sensitivity to tropopause height. *Journal of the Atmospheric Sciences*, *63*, 1954–1961.
Yuval, J., & Kaspi, Y. (2020). Eddy activity response to global warming-like temperature changes. *Journal of Climate*, *33*(4), 1381–1404. https://doi.org/10.1175/JCLI-D-19-0190.1